Rational Design of Two-Dimensional Nanoscale Networks by Electrostatic Interactions at Surfaces

Sebastian Stepanow,[†,*] Robin Ohmann,[†] Frederic Leroy,[†,#] Nian Lin,[†,∥] Thomas Strunskus,[‡,▽] Christof Wöll,[‡,§] and Klaus Kern[†,⊥]

[†]Max-Planck-Institut für Festkörperforschung, Heisenbergstrasse 1, D-70569 Stuttgart, Germany, [‡]Lehrstuhl für Physikalische Chemie I, Ruhr-Universität Bochum, D-44780 Bochum, Germany, [§]Institut für Oberflächenchemie, Karlsruhe Institut für Technologie, D-76021 Karlsruhe, Germany, [⊥]Institut de Physique de la Matière Condensée, Ecole Polytechnique Fédérale de Lausanne, CH-1015 Lausanne, Switzerland, and [∥]Department of Physics, The Hong Kong University of Science and Technology, Clear Water Bay, Kowloon, Hong Kong, China. [#]Current address: CNRS-Aix-Marseille Universite, CINaM-UPR 3118, Campus de Luminy, case 913, F-13288 Marseille cedex, France. [▽]Current address: Institut für Materialwissenschaft - Materialverbunde, Technische Fakultät, Christian-Albrechts-Universität Kiel, D-24118 Kiel, Germany.

ABSTRACT The self-assembly of aromatic carboxylic acids and cesium adatoms on a Cu(100) surface at room temperature has been investigated by scanning tunneling microscopy and X-ray photoelectron spectroscopy. The highly ordered molecular nanostructures are comprised of a central ionic coupling motif between the anionic carboxylate moieties and Cs cations that generate distinctive chiral arrangements of the network structures. The primary electrostatic interaction results in highly flexible bond lengths and geometries. The adsorbate—substrate coupling is found to be important for the determination of the structures. With the use of rod-like carboxylic linker molecules, the dimension of the porous networks can be tuned through the variation of the aromatic backbone length.

KEYWORDS: ionic self-assembly · scanning tunneling microscopy · molecular nanostructures · chirality · supramolecular chemistry · XPS · UHV

Bottom-up fabrication of two-dimensional periodic molecular nanostructures has gained extensive attention recently.[1,2] Concepts of supramolecular chemistry have been successfully employed to attain nanostructures supported at surfaces providing programmable topology *via* supramolecular assembly.[3−11] Specific intermolecular interactions, *e.g.*, hydrogen bonds, metal coordination, and van der Waals forces, have been used to link constituting building blocks. Also, interactions between polar regions of a molecule have been identified to steer molecular organizations.[12] Recently, ionic self-assembly was introduced to fabricate supramolecular functional materials in wet chemical environments including liquid crystals as well as fibers and nanotubes.[13] The ionic self-assembly process uses electrostatic interactions between oppositely charged molecular species as the primary interaction. This method has become a powerful tool to fabricate nanostructured materials with unique structural and chemical properties.[13−16] The advantage of this method lies in its simplicity, flexibility, and the wide availability of the building components. Here, we demonstrate that ionic self-assembly can be employed as a simple and versatile method to achieve rational design of two-dimensional nanostructures at metal surfaces in solvent-free "dry" ultrahigh vacuum conditions.

As building blocks, we choose carboxylic acids and alkali metal atoms, both known to be easily found in solutions in their anionic and cationic state, respectively. In the first case, this behavior is related to the acidity of the molecules donating easily their carboxylic hydrogen. In the latter case the relatively low electronegativity and ionization potential of alkali metals results in electron donation from the outer *s*-shell, leaving the ion in a stable rare gas configuration. Scheme 1 shows the molecular formula of four organic molecules used in the present study, polybenzene dicarboxylic acids, 1,4-benzoic acid (terephthalic acid, TPA), 4,4′-biphenyldicarboxylic acid (BDA), 4,1′,4′,1′′-terphenyl-1,4′′-dicarboxylic acid (TDA), and 2,2′-bipyridine-5,5′-dicarboxylic acid (BPyDA). Their common structural feature comprises a linear aromatic backbone and two carboxyl groups at both ends, at a distance of 7.1, 11.4, 15.7, and 11.4 Å, respectively. It will be shown in the next paragraphs that the ionic character of the components emerges upon adsorption at a metal surface.

*Address correspondence to s.stepanow@fkf.mpg.de.

Received for review August 10, 2009 and accepted March 17, 2010.

Published online March 25, 2010.
10.1021/nn100303z

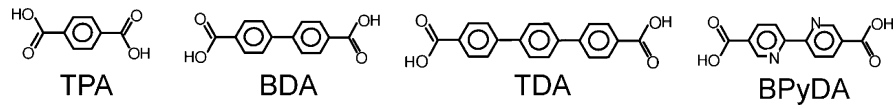

Scheme 1. Molecular formulas of the four organic linkers used in the present study.

At the surface the aromatic backbone of the organic molecules ensures a flat-lying adsorption geometry, *i.e.*, with the aromatic rings parallel to the surface.[7,17] The carboxyl groups deprotonate when the molecules adsorb at the Cu(100) surface under the employed experimental conditions, which was demonstrated by X-ray photoelectron spectroscopy (XPS) and Fourier transform infrared spectroscopy (FTIRS) measurements in earlier studies.[17,18] The charge state of the carboxylate group was also investigated for a related aromatic polycarboxylic acid adsorbed on a metal surface by *ab initio* calculations based on density functional theory. The theoretical modeling estimated a charge accumulation of about −0.6e *per* deprotonated carboxylic group with a charge distribution localized at the oxygen atoms of the carboxylate moiety.[19] Hereafter, the abbreviations TPA, BDA, TDA, and BPyDA refer to the deprotonated ionic species.

In our study, the oppositely charged component is represented by Cs adatoms. The adsorption of the strongly electropositive alkali metals on semiconducting and metal surfaces lowers the work function substantially. The minimum of the work function is found roughly at a coverage of half monolayer with a value below the corresponding bulk alkali metal work function.[20−23] These observations, further investigated by more sophisticated experimental and theoretical methods,[24−27] have been explained by the broadening of the outer *s*-state and partial charge transfer to the metal surface. Thereby, the alkali metal becomes partly ionic and reduces the work function. Model cluster calculations estimate the charge transfer from Cs to the supporting Cu surface to be about −0.4e.[26] Hence, the Cs atoms adsorbed at the metal surface can be regarded as cations. This also accounts for the substantial repulsive lateral interactions between the Cs adatoms preventing the formation of metal clusters at the initial stage of growth.[20,21] The latter behavior is in contrast to transition metal atoms employed in previous studies and represents an advantage for the formation of multicomponent molecular nanostructures.[5,7]

The linkers carrying carboxylate anions and the Cs cations represent complementary components for the attractive ionic coupling, which is found in the corresponding bulk materials. At the metal surface, the ionic species will be screened by the conduction electrons, thus, creating oppositely oriented standing dipoles for the two components. Despite the screening, the primary interaction between the constituents is still of an electrostatic nature. Here we show that the proposed coupling motif between carboxylate moieties and Cs adatoms can be used to steer the molecular organization at a metal surface and fabricate well-defined structures whose dimensions can be controlled by the length of the aromatic backbone.

RESULTS AND DISCUSSION

Upon deposition of molecules and Cs atoms onto the Cu(100) surface, various ordered phases were observed depending on the molecule-to-Cs concentration

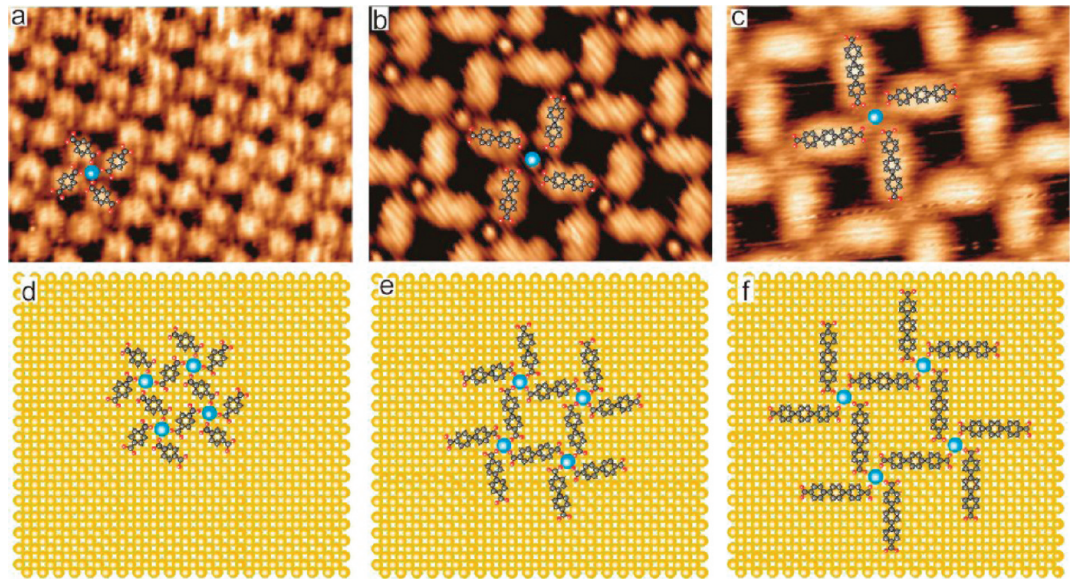

Figure 1. STM topograph of (a) TPA-, (b) BDA-, and (c) TDA-Cs networks. Image size: 5.8 × 7.8 nm. (d−f) Models of the three networks. All constituents are assumed to reside in the same plane parallel to the surface and the Cs ions occupy the substrate hollow sites. The Cs ions form superstructures of [2, 4/−4, 2], [5, 3/−3, 5], and [7, 3/−3, 7] in the TPA, BDA, and TDA networks, respectively.

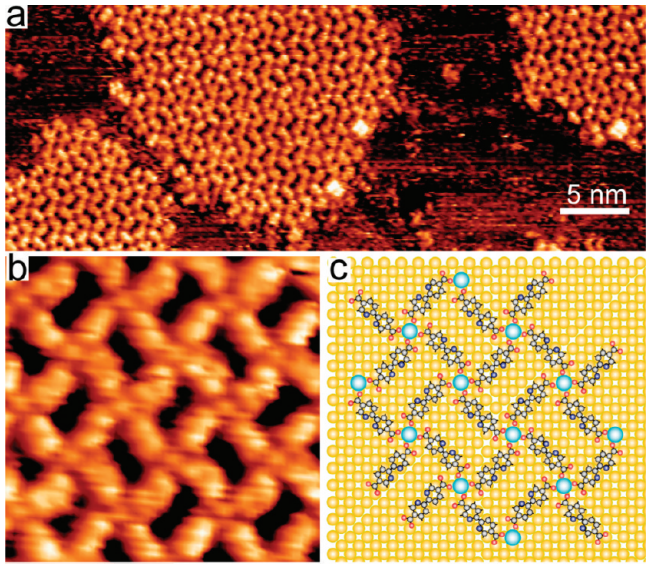

Figure 2. BPyDA-Cs network: (a) Overview STM topograph; (b) Detail STM topograph showing the chessboard arrangement of the 90°-rotated rectangular voids. Image size: 6.3 × 6.5 nm. (c). A model illustrating that the two chiral binding motifs organize alternatingly, resulting in an achiral network.

ratio. At proper molecule and Cs concentrations, the mixture of organic linkers and alkali metal adatoms self-assemble into open two-dimensional square network structures. Figure 1a−c and Figure 2 reproduce typical STM topographs of the network structures of the TPA, BDA, TDA, and BPyDA molecules, respectively, in which the molecular linkers and Cs atoms are clearly resolved. All four molecules organize with Cs as networks containing square-shaped voids. Besides the open network structures discussed here, a variety of other ordered phases with relatively complicated unit cells are presented in Figures S1 and S2 for TPA and BDA and Figure S3 for trimesic acid (TMA) in the Supporting Information. All structures appear to be stable at room temperature, although fuzzy domain edges and partial reshaping of domains while scanning as well as spikes in open substrate areas are indicative of the presence of rapidly diffusing adsorbates, see, *e.g.*, Figure S1a. This means that the condensed structures are in equilibrium with gas-like entities.

The models superimposed on the data in Figure 1 display a common structural feature of the four networks in Figures 1 and 2, *i.e.*, four linker molecules point to a central Cs atom. We propose that this structural configuration is stabilized by ionic interactions between the positively charged Cs and the negatively charged carboxylate end groups. The total charge of the four carboxylates and the central Cs is elusive because the influence of the metal substrate must be taken into account, which effectively screens the charged adsorbates. Before we proceed to the detailed description of the molecular organizations we present the analysis of the chemical nature of the adsorbates.

To obtain information on the chemical state of the molecules and Cs atoms, we carried out XPS measurements. Figure 3 summarizes the results obtained for the BPyDA system in the presence and absence of Cs adatoms. In Figure 3a, the oxygen 1s XPS data is presented for a BPyDA submonolayer after annealing to 400 K with (lower curve) and without coadsorption of Cs (middle curve). In addition, the spectrum for a BPyDA multilayer deposited at room temperature is shown (upper curve in Figure 3a). The spectrum of the multilayer shows a broad peak that can be decomposed into two contributions by fitting with Gaussian peaks centered at 532.25 and 534.2 eV, which we attribute to the oxygen atoms in the carbonyl (-C═O) and hydroxyl (-C−OH) groups, respectively, in accordance with earlier observations.[17] The submonolayer of BPyDA exhibits only a single peak with a binding energy of 531.2 eV corresponding to the chemically equivalent oxygen atoms in the carboxylate moiety.[17] Thus, the molecules directly in contact with the copper surface are deprotonated under the employed experimental conditions. Upon Cs addition, the position of the peak is subjected

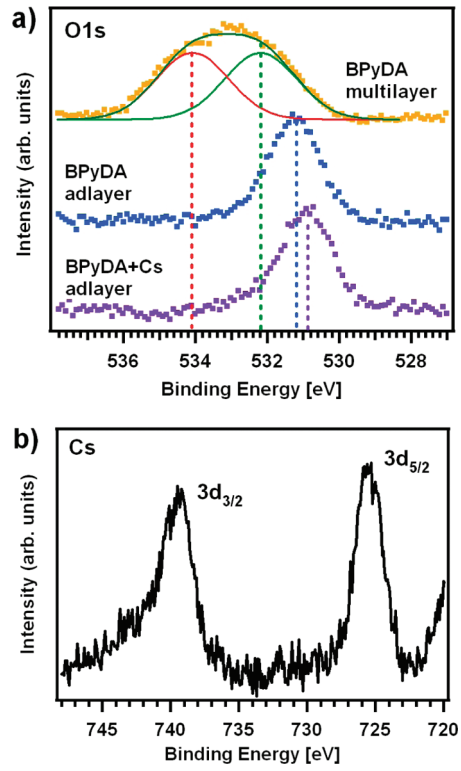

Figure 3. XPS data of BPyDA molecules and Cs adatoms on Cu(100). (a) Oxygen 1s core level photoemission spectra of BPyDA in the mono- and multilayer regime as well as in the presence of Cs atoms on the surface. Vertical lines mark the binding energies of the chemically different oxygen atoms. (b) Cesium 3d photoemission spectrum for Cs atoms deposited on a BPyDA submonolayer.

to a small shift of 0.3 eV to a lower binding energy of 530.9 eV. In comparison, an energy shift of 0.6 eV toward higher binding energies was found for the oxygen 1s peak in the carboxylate coordination networks with Fe centers that is opposite to the Cs networks presented here.[28] We attribute these findings to the different bonding mechanisms involved in these systems. The metal coordination bond (Fe−O) has a significant orbital overlap between the oxygen atoms and the Fe centers accompanied by charge redistribution that differs from primary electrostatic interactions.

Figure 3b shows XPS data obtained at the Cs(3d) region corresponding to the oxygen 1s spectrum for the BPyDA+Cs data in Figure 3a. The spectrum exhibits narrow single peaks signifying that the Cs adatoms are present in equivalent chemical states. The binding energy of the $Cs3d_{5/2}$ peak amounts to 725.5 eV. This value lies in between that for metallic cesium(0) at 726.3 eV[29] and for Cs in bulk systems with a formal charge of +1 with reported values of 723.5−724 eV.[30] Similar binding energies were observed for Cs on a clean (725.6 eV) and oxygen covered (725.1 eV) Cu(110) surface.[31] This observation suggests that the Cs atoms are partially positively charged, in line with the theoretical investigations.

The XPS measurements demonstrate that the anionic carboxylate groups are slightly altered toward more negative character in the presence of Cs adatoms compared to the pristine molecular phase and, moreover, that the Cs adatoms at low concentrations and incorporated in the molecular networks exhibit a shift in binding energy that is indicative of partial charge transfer from the Cs atom. Both results support the scenario of ionic coupled molecular arrays.

A closer inspection of the STM images in Figure 1 reveals details of the binding scheme. The common feature at the network nodes is that the four linkers do not point to the central Cs symmetrically but rather tilt to one side. In addition, all four linkers tilt to the same direction and the second O atom of the carboxylate group potentially forms a hydrogen bond to the adjacent molecule, which generates a propeller arrangement; see also Figures S2 and S3 in the Supporting Information. Propeller structures were also observed for the Fe−TPA coordination complexes assembled at surfaces.[5] Similar to the Fe-carboxylate complexes, these propellers represent two-dimensional chiral species, *i.e.*, the four linkers are folded either clockwise or counterclockwise with respect to the central Cs, which can not be superimposed to each other by in-plane rotations or displacements. Therefore, the binding motifs comprise chiral information.

The continuous extension of the binding motif provided by the two equal binding sites of the linker molecules results in extended two-dimensional networks. Single network domains of BDA and TDA can grow as large as 50 nm, whereas the domain size of this particular TPA network structure is smaller (≈10 nm). A larger Cs-TPA domain of a different structure can be seen in Figure S1a. Based on the STM analysis, the Cs ions in the TPA, BDA, and TDA networks organize as square lattices that are consistent with the commensurate superstructures defined by [2, 4/−4, 2], [5, 3/−3, 5], and [7, 3/−3, 7], respectively. The formation of the well-defined superstructures suggests that besides the ionic coupling scheme the surface also plays a significant role in the determination of the network structures. Due to the adsorbate−substrate coupling, the molecular species and the Cs ions prefer certain adsorption sites and molecular orientations with respect to the substrate atomic lattice. The overall network structure is thus determined by the balance between the ionic and the substrate−adsorbate interactions. The periodicity and orientation of the networks with respect to the Cu(100) surface are rationalized by the models shown in Figure 1d−f, where we assume that all constituents reside in the same plane parallel to the surface and the Cs ions occupy the substrate hollow sites. The molecular geometries in the model were calculated for isolated molecules in the PM3 approximation.[32] A DFT calculation shows that the C−C bond relaxation of chemisorbed benzene on a Cu(100) surface results in an increased bond length of less than 2% and can be neglected for the determination of intermolecular distances.[33] Therefore, we use an unrelaxed molecular and surface geometry in our models. The oxygen−Cs distances obtained from the models in Figure 1d−f and Figure 2c vary from 2.2 ± 0.2 Å for BDA−Cs to 2.7 ± 0.2 Å for TDA−Cs. The broad variance of the oxygen−Cs distances is attributed to the influence of the substrate and signifies the flexibility of the electrostatic interactions, *i.e.*, the bond length variation is considerably larger than in transition-metal coordination compounds for the same type of molecular ligands.[7]

Figure 1a−c shows that the single network domains consist of pure enantiomeric binding motifs, resulting in homochiral phases. The domains of mirror reflection are also encountered elsewhere on the surface, thus the networks form a racemic conglomerate. Figure 4 shows an STM image containing several BDA network domains. Note that there exist two different network orientations with respect to the substrate. A detailed analysis reveals that they are two enantiomeric phases of the homochiral domains in which the folding of the BDA linkers relative to the central Cs is mirrored, as illustrated by the corresponding models. Besides the two enantiomeric pure homochiral phases, the TDA linker forms another network phase that has not been observed for TPA or BDA. As shown in Figure 5a, a homochiral network domain that contains square voids is located at the lower-left part, whereas at the upper-right part a network consisting of elongated rectangular voids is present. A close inspection of this structure reveals that the propeller arrangement of the link-

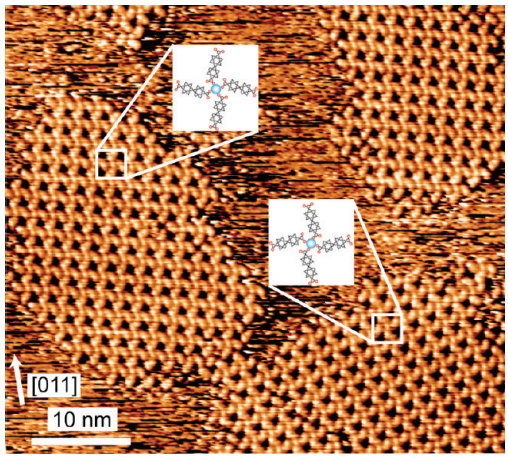

Figure 4. Overview of the BDA networks showing the two types of homochiral domains. Insets show the models of the two enantiomeric binding motifs, in which the linkers are folded oppositely around the central Cs atom.

ers at adjacent Cs ions is opposite to each other and alternates between the network nodes. The major difference to the homochiral phase is given by the coexistence of both enantiomers of the chiral binding motif, thus, rendering the network domain achiral. In Figure 5b, a model for the achiral TDA phase is presented, the networks can be described as a (10 × 10) superstructure with respect to the substrate lattice consistent with STM observations. The model also rationalizes the appearance and the alternating arrangement of the 90° rotating rectangular voids in which the alternation of the two enantiomeric propeller arrangements is shown explicitly.

The coexistence of the two phases suggests that the two different chiral organizations are very close in energy. As seen in Figure 1f, the TDA molecules align with the high-symmetry directions of the substrate lattice, *i.e.*, the reflection does not alter the adsorption configuration. Thus, both enantiomeric phases of the homochiral networks comprise TDA with the same adsorption configuration. The coexistence of homochiral and achiral domains can be rationalized with the following. When the models presented in Figures 1f and 5b are considered, the TDA and Cs in the two different network structures reside at exactly the same adsorption sites resulting in identical bond lengths between Cs and the carboxylate oxygen. The very same adsorption configuration and binding motifs indicates that the achiral network is energetically equal to the homochiral network. The same argument can explain why the achiral phase is absent for TPA and BDA networks. In contrast to TDA, the TPA or BDA molecules do not align along the principal substrate directions in the homochiral phases (*cf.* Figure 1d and e). To form the achiral network for the TPA or BDA molecules, a certain amount of constituting molecules or Cs ions must adsorb differently at the substrate to maintain the binding distance of oxygen-to-Cs, *i.e.*, at sites or of orientations that significantly deviate from those of the energetically favored configurations encountered in the homochiral phase. Therefore, an achiral TPA or BDA network is energetically unfavorable.

The different expression of chirality for different molecules hints in principle that one may steer chiral organizations by tuning substrate−adsorbate interactions. To test this idea, we have used the BPyDA molecule, which is geometrically identical to BDA but with nitrogen substitutions at the 2 and 2′ positions of the aromatic backbone. As shown in Figure 2a, only one type of BPyDA network domain has been observed. The close-view of the network reproduced in Figure 2b reveals that it possesses similar structural features as the achiral phase of the TDA network, *i.e.*, clockwise folding and counter-clockwise folding of the molecules occurs alternatingly at the network nodes giving two types of 90° rotated rectangular voids that are arranged in a chessboard pattern. Therefore, the BPyDA-Cs domains are achiral, which is distinctively different from the geometrically identical BDA. This difference is ascribed to the specific adsorption configuration of pyridine and benzene units at the surface.[34] It was reported that the N-substitution in pyridine contributes significantly, even predominantly to the substrate−adsorbate binding.[35] Our studies of the pure BPyDA adlayers on Cu(100) indicate that BPyDA adsorbs almost flat lying at the present experimental conditions, with both substituted N atoms presumably residing on top sites of the Cu(100) surface.[36] Figure 2c shows a model illustrating the supramolecular organization and the resulting alternating arrangements of rectangular voids. In this

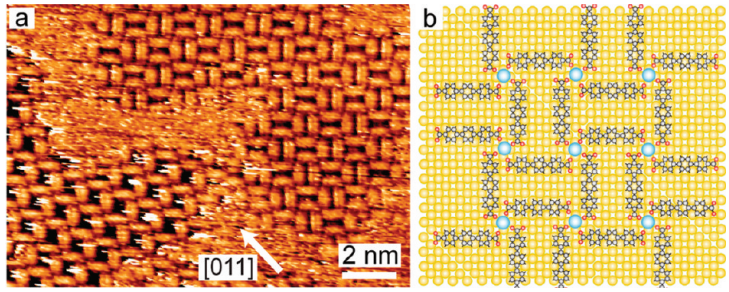

Figure 5. (a) Coexistence of a homochiral (lower-left) and an achiral (upper-right) domain of the TDA networks. (b) Model illustrating the alternation of the two chiral binding motifs in the achiral phase. Formation and arrangement of the elongated voids is also expressed.

model, BPyDA is oriented along the high-symmetry substrate directions. Apparently, this molecular orientation allows forming an achiral network phase, as encountered in the corresponding TDA phase. Based on the asymmetric shape of the BPyDA molecules in the STM topograph, we propose that they adsorb in the *cis*-conformation. A detailed study of the conformation of the BPyDA will be reported elsewhere. It is worthwhile to point out that the aromatic backbone (N atoms) functionalizes the cavity additionally which could be used to bind additional species allowing for more complex hierarchical structures. The selective interaction of the Cs atoms with the carboxylate functionalities demonstrates that the bonding favors the strongly polarized groups.

The presented coupling scheme produces highly ordered molecular arrays where the organization can be steered by the backbone functionality of the organic linkers. Compared to metal coordination systems reported earlier this approach differs in several key features.[7] The directionality and strength of the transition metal coordination is determined by the involved atomic and molecular orbitals as well as the σ-donation and π-back-donation character of the ligands, however, this information is lost in the ionic alkali-salt systems. Furthermore, the bond length specificity differs considerably. While metal coordination interactions result in a narrow range bond length distribution, the presented coupling scheme shows a much larger variation, and therefore, the molecules can readily adapt the registry imposed by the supporting surface. Another advantage lies in the simplified preparation procedure which requires substantially lower substrate temperatures. The Fe coordinated carboxylate structures require an annealing at 400−450 K for proper reticulation, whereas the preparation of the Cs−carboxylate networks is carried out at room temperature. Furthermore, transition metal adatoms tend to form stable cluster at surfaces, which are then lost for the metal−organic network formation. However, the repulsive interaction of Cs prevents the irreversible formation of metal clusters at low concentrations, which allows for the reversal of the deposition sequence of the components without loss of control for the structure determination. In contrast to metal coordination compounds at surfaces, the presented ionic coupled networks are less stable at room temperature, as evidenced by the presence of mobile species on the surface and the mobility at the network edges in subsequently taken STM images. The high mobility of adsorbates and continuous reshaping of network domains evidenced by fuzzy domain edges and spikes in open surfaces areas is also apparent in Figures 4a and 5a. This behavior points to a comparatively weak bond strength and is related to partially ionized species and charge screening by the metal substrate. The screening will also affect the long-range character of the interaction. Thus, the effective interaction length will be of the order of the screening length of the metal substrate, *i.e.*, a few Angstrom. However, it has been shown that for positively charged donor molecules at a Au(111) surface the repulsive interaction can be effective up to a few nanometers.[37] Hence, the presented interaction is of intermediate strength compared to hydrogen bonding and metal coordination and could be used for the fabrication of hierarchical structures with higher complexity.

CONCLUSIONS

In conclusion, we have demonstrated that self-assembly driven by primary electrostatic interactions can be successfully applied to fabricate two-dimensional nanoporous networks at a metal surface. The dimensions of the networks are determined by the backbone length of the linker molecules. The substrate influence is expressed by the fact that distinctive chiral organizations evolve depending on the balance of the adsorption strength and the electrostatic interactions. Because the electrostatic interactions are very flexible and widely encountered, the reported method represents an easy route to assemble two-dimensional periodic nanostructures at surfaces. In particular, because molecules carrying charged end groups, *e.g.*, proton acceptor or donor moieties, and other atomic and molecular electron donor and acceptor species, are abundantly available, we believe that this technique may find general application in the bottom-up fabrication of low-dimensional molecular nanostructures.

METHODS

STM. The sample preparation and STM measurements were carried out in an ultrahigh-vacuum (UHV) chamber with a base pressure of 2×10^{-10} mbar, providing well-defined conditions for the experiments. The UHV chamber is equipped with standard facilities for surface preparation. The Cu(100) surface was prepared by repeated cycles of argon ion sputtering and subsequent annealing to 800 K. The organic linker molecules and the Cs atoms were consecutively deposited onto the Cu(100) surface. The organic linker molecules TPA (Fluka Chemie AG, purity >99%), BDA (Sigma-Aldrich, purity 97%), BPyDA (Fluka Chemie AG, purity 97%), TMA (Sigma-Aldrich, purity >99%), and the specially synthesized TDA molecule,[38] all in powder form, were evaporated from a resistively heated crucible held at a specific temperature. The molecules were sublimed at 440, 490, 520, 460, and 530 K for TPA, BDA, BPyDA, TMA, and TDA, respectively, with evaporation rates in the order of a tenth of a monolayer per minute. Before the experiments, the molecules were thoroughly degassed at a temperature 10 K below the sublimation temperature. During evaporation the Cu(100) substrate was held above 300 K. For the organic precursor layers, the coverage was kept below a full monolayer to provide the necessary mobility of the molecules and space for the formation of networks. Cs atoms were subsequently deposited using an alkali metal dispenser (SAES Getters) onto the substrate held at a temperature ranging from 300 to 360 K. The order of the evaporation of the

constituents does not matter for the formation of the networks. Calibration of the Cs coverage was not feasible by STM due to the high mobility of the alkali adatoms on Cu(100) and the absence of cluster formation. However, a general estimation of the ratio between the linker molecules and the Cs atoms gives roughly the stoichiometric composition of 2:1 to obtain the network structures. The organic molecules TPA, BDA, and BPyDA form a variety of structures different from the networks presented here, which depend strongly on the metal-to-molecule ratio. Some of these structures are shown in the Supporting Information. For all systems, no structural transitions have been observed upon annealing to 400 K and cooling to room temperature for STM imaging. The STM images were acquired at room temperature in the constant current mode with bias voltages in the range from a few mV up to 1.5 V and a tunneling current of 0.1 nA in the same UHV chamber.

XPS. The X-ray photoelectron spectroscopy (XPS) measurements were carried out at the HE-SGM beamline at the Berlin synchrotron radiation facility BESSY II. The analysis chamber (base pressure better than 2×10^{-10} mbar) was equipped with standard facilities for sample preparation, a quadrupole mass spectrometer, as well as a twin anode X-ray source and a CLAM2 energy analyzer. The samples were prepared *in situ*, following the procedures established in the STM experiments. The XPS data for the oxygen 1s as well as carbon 1s and nitrogen 1s peak (the latter two not shown here) were acquired with a beam energy of 650, 400, and 450 eV, respectively. The pass energy of the analyzer was set to 50 eV. For quantitative analysis, a complete set of XP spectra including the cesium 3d peaks was acquired in addition with the Al K_α radiation of the laboratory source with a pass energy set to 100 eV. All data was acquired with the sample at room temperature. The spectra have been referenced to the Cu $3p_{3/2}$ or Cu $2p_{3/2}$ line at 75.1 and 932.7 eV, respectively. The BPyDA-to-Cs concentration ratio was roughly estimated by the ratio of the integrated intensities of the carbon 1s and cesium $3d_{5/2}$ XPS peaks normalized to the atomic sensitivity factors according to Scofield. The ratio is about 1:1.6 for the presented data. Higher Cs concentrations do not change the oxygen 1s or cesium 3d spectra.

Acknowledgment. We thank Chengzhi Cai for providing the TDA molecules.

Supporting Information Available: STM images of other ordered Cs-molecule phases on the Cu(100) surface are provided for the TPA, BDA, and TMA (trimesic acid) molecules. This material is available free of charge *via* the Internet at http://pubs.acs.org.

REFERENCES AND NOTES

1. Barth, J. V.; Costantini, G.; Kern, K. Engineering Atomic and Molecular Nanostructures at Surfaces. *Nature* **2005**, *437*, 671–679.
2. Shchukin, V. A.; Bimberg, D. Spontaneous Ordering of Nanostructures on Crystal Surfaces. *Rev. Mod. Phys.* **1999**, *71*, 1125–1171.
3. De Feyter, S.; Gesquiére, A.; Klapper, M.; Müllen, K.; De Schryver, F. C. Toward Two-Dimensional Supramolecular Control of Hydrogen-Bonded Arrays: The Case of Isophthalic Acids. *Nano Lett.* **2003**, *3*, 1485–1488.
4. Yan, H.; Park, S. H.; Finkelstein, G.; Reif, J. H.; LaBean, T. H. DNA-Templated Self-Assembly of Protein Arrays and Highly Conductive Nanowires. *Science* **2003**, *301*, 1882–1884.
5. Lin, N.; Stepanow, S.; Ruben, M.; Barth, J. V. Surface-Confined Supramolecular Coordination Chemistry. *Top. Curr. Chem.* **2009**, *287*, 1–45.
6. Yokoyama, T.; Yokoyama, S.; Kamikado, T.; Okuno, Y.; Mashiko, S. Selective Assembly on a Surface of Supramolecular Aggregates with Controlled Size and Shape. *Nature* **2001**, *413*, 619–621.
7. Stepanow, S.; Lin, N.; Barth, J. V.; Kern, K. Surface-Template Assembly of Two-Dimensional Metal-Organic Coordination Networks. *J. Phys. Chem. B* **2006**, *110*, 23472–23477.
8. Yokoyama, T.; Kamikado, T.; Yokoyama, S.; Mashiko, S. Conformation Selective Assembly of Carboxyphenyl Substituted Porphyrins on Au(111). *J. Chem. Phys.* **2004**, *121*, 11993–11997.
9. Theobald, J. A.; Oxtoby, N. S.; Phillips, M. A.; Champness, N. R.; Beton, P. H. Controlling Molecular Deposition and Layer Structure with Supramolecular Surface Assemblies. *Nature* **2003**, *424*, 1029–1031.
10. Stepanow, S.; Lingenfelder, M.; Dmitriev, A.; Spillmann, H.; Delvigne, E.; Lin, N.; Deng, X.; Cai, C.; Barth, J. V.; Kern, K. Steering Molecular Organization and Host-Guest Interactions Using Two-Dimensional Nanoporous Coordination Systems. *Nat. Mater.* **2004**, *3*, 229–233.
11. Langner, A.; Tait, S. L.; Lin, N.; Rajadurai, C.; Ruben, M.; Kern, K. Self-Recognition and Self-Selection in Multicomponent Supramolecular Coordination Networks on Surfaces. *Proc. Natl. Acad. Sci. U.S.A.* **2007**, *104*, 17927–17930.
12. Kuck, S.; Chang, S.-H.; Klöckner, J.-P.; Prosenc, M. H.; Hoffmann, G.; Wiesendanger, R. Steering Two-Dimensional Molecular Growth via Dipolar Interaction. *Chem. Phys. Chem.* **2009**, *10*, 2008–2011.
13. Faul, C. F. J.; Antonietti, M. Ionic Self-Assembly: Facile Synthesis of Supramolecular Materials. *Adv. Mater.* **2003**, *15*, 673–683.
14. Zhang, T.; Spitz, C.; Antonietti, M.; Faul, C. F. J. Highly Photoluminescent Polyoxometaloeuropate-Surfactant Complexes by Ionic Self-Assembly. *Chem.—Eur. J.* **2005**, *11*, 1001–1009.
15. Zakrevskyy, Y.; Smarsly, B.; Stumpe, J.; Faul, C. F. J. Highly Ordered Monodomain Ionic Self-Assembled Liquid-Crystalline Materials. *Phys. Rev. E* **2005**, *71*, 021701.
16. Wang, Z.; Medforth, C. J.; Shelnutt, J. A. Porphyrin Nanotubes by Ionic Self-Assembly. *J. Am. Chem. Soc.* **2004**, *126*, 15954–15955.
17. Stepanow, S.; Strunskus, T.; Lingenfelder, M.; Dmitriev, A.; Spillmann, H.; Lin, N.; Barth, J. V.; Wöll, C.; Kern, K. Deprotonation-Driven Phase Transformations in Terephthalic Acid Self-Assembly on Cu(100). *J. Phys. Chem. B* **2004**, *108*, 19392–19397.
18. Chen, Q.; Perry, C. C.; Frederick, B. G.; Murray, P. W.; Haq, S.; Richardson, N. V. Structural Aspects of the Low-Temperature Deprotonation of Benzoic Acid on Cu(110) Surfaces. *Surf. Sci.* **2000**, *446*, 63–75.
19. Ruben, M.; Payer, D.; Landa, A.; Comisso, A.; Gattinoni, C.; Lin, N.; Collin, J.-P.; Sauvage, J.-P.; De Vita, A.; Kern, K. 2D Supramolecular Assemblies of Benzene-1,3,5-triyl-tribenzoic Acid: Temperature-Induced Phase Transformations and Hierarchical Organization with Macrocyclic Molecules. *J. Am. Chem. Soc.* **2006**, *128*, 15644–15651.
20. Papageorgopoulos, C. A. Studies of Separate Adsorption and Coadsorption of Cs and O_2 on Cu(100). *Phys. Rev. B* **1982**, *25*, 3740–3750.
21. Bonzel, H. P. Alkali-Metal-Affected Adsorption of Molecules on Metal Surfaces. *Surf. Sci. Rep.* **1987**, *8*, 43–125.
22. Lang, N. D. Theory of Work-Function Changes Induced by Alkali Adsorption. *Phys. Rev. B* **1971**, *4*, 4234–4244.
23. Gurney, R. W. Theory of Electrical Double Layers in Adsorbed Films. *Phys. Rev.* **1935**, *47*, 479–482.
24. Woratschek, B.; Sesselmann, W.; Küppers, J.; Ertl, G.; Haberland, H. 4s Valence Level of Adsorbed K Atoms Probed by Metastable-He Deexcitation Spectroscopy. *Phys. Rev. Lett.* **1985**, *55*, 1231–1234.
25. Ishida, H. Theory of the Alkali-Metal Chemisorption on Metal Surfaces. II. *Phys. Rev. B* **1990**, *42*, 10899–10911.
26. Gao, S.; Wang, D. An Embedding Scheme for Calculating Charge Transfer between Adsorbates and Metal Surfaces. *J. Phys.: Condens. Matter* **1990**, *2*, 2187–2198.
27. Bagus, P. S.; Käfer, D.; Witte, G.; Wöll, C. Work Function Changes Induced by Charged Adsorbates: Origin of the Polarity Asymmetry. *Phys. Rev. Lett.* **2008**, *100*, 126101.
28. Tait, S. L.; Wang, Y.; Costantini, G.; Lin, N.; Baraldi, A.; Esch, F.; Petaccia, L.; Lizzit, S.; Kern, K. Metal-Organic Coordination Interactions in Fe-Terephthalic Acid

Networks on Cu(100). *J. Am. Chem. Soc.* **2008**, *130*, 2108–2113.
29. Ebbinghaus, G.; Simon, A. Electronic Structure of Rb, Cs and Some of Their Metallic Oxides Studied by Photoelectron Spectroscopy. *Chem. Phys.* **1970**, *43*, 117–133.
30. Wagner, C. D.; Riggs, W. M.; Davis, L. E.; Moulder, J. F. In *Handbook of Photoelectron Spectroscopy*; Muilenberg, G. E. , Ed.; Physical Electronics Division, Perkin-Elmer Corp.: Eden Prairie, MN, 1979.
31. Carley, A. F.; Davies, P. R.; Harikumar, K. R.; Jones, R. V.; Roberts, M. W. Reactivity and Structural Aspects of Cesium and Oxygen States at Cu(110) Surfaces: An XPS and STM Investigation. *J. Phys. Chem. B* **2004**, *108*, 14518–14526.
32. Dewar, M. J. S.; Zoebisch, E. G.; Healy, E. F.; Stewart, J. J. P. AM1: A New General Purpose Quantum Mechanical Molecular Model. *J. Am. Chem. Soc.* **1985**, *107*, 3902–3909.
33. Lorente, N.; Hedouin, M. F. G.; Palmer, R. E.; Persson, M. Chemisorption of Benzene and STM dehydrogenation Products on Cu(100). *Phys. Rev. B* **2003**, *68*, 155401.
34. Bilić, A.; Reimers, J. R.; Hush, N. S. Adsorption of Pyridine on the Gold(111) Surface: Implications for "Alligator Clips" for Molecular Wires. *J. Phys. Chem. B* **2002**, *106*, 6740–6747.
35. Haq, S.; King, D. A. Configurational Transitions of Benzene and Pyridine Adsorbed on Pt(111) and Cu(110) Surfaces: An Infrared Study. *J. Phys. Chem.* **1996**, *100*, 16957–16965.
36. Ohmann, R. Rastertunnelmikroskopie und -spektroskopie an molekularen Nanostrukturen. Diploma thesis, University Konstanz, Germany, 2005.
37. Fernandez-Torrente, I.; Monturet, S.; Franke, K. J.; Fraxedas, J.; Lorente, N.; Pascual, J. I. Long-Range Repulsive Interaction between Molecules on a Metal Surface Induced by Charge Transfer. *Phys. Rev. Lett.* **2007**, *99*, 176103.
38. Campbell, T. W. Dicarboxylation of Terphenyl. *J. Am. Chem. Soc.* **1960**, *82*, 3126–3128.